

Average Absorption Coefficient Measurement of Arbitrarily Shaped Electrically Large Objects in a Reverberation Chamber

Qian Xu, Yi Huang, *Senior Member, IEEE*, Lei Xing, Zhihao Tian, Jiafeng Zhou, Anqi Chen and Yuan Zhuang

Abstract—It is shown in this letter that the average absorption coefficient (AAC) of an object under test (OUT) can be obtained by comparing the measured absorption cross section (ACS) of the OUT with the ACS value of a perfect absorber of the same shape. The ACS of an arbitrarily shaped electrically large perfect absorber can be obtained numerically. Measurements are performed to demonstrate the proposed method. Results show that the AAC is not sensitive (but not independent) to the shape and size of an electrically large absorber. The procedure proposed in this letter can be used to characterize the electromagnetic wave absorptive and scattering ability of arbitrarily shaped objects. A system-level AAC could be very useful for many applications.

Index Terms—absorption cross section, absorption coefficient, reverberation chamber.

I. INTRODUCTION

THE absorption cross section (ACS) measurement in a reverberation chamber (RC) has been widely studied [1]-[11]. The ACS depends on the shape and material properties of an object under test (OUT) [11]. The ACS of a given object can be measured in the RC; however, if we want to characterize the material of the object, the size and shape of the object need to be considered. A big OUT with small losses could have the same ACS value as an OUT with a smaller size but higher losses. It is worth mentioning that if the OUT is planar, the average absorption/scattering coefficient can be obtained by comparing the ACS value to an ideal absorber with the same size [12]-[14]. If this method can be generalized to an arbitrarily shaped OUT measurement, it could be very useful for applications such as material characterization, microwave absorption of a human body, predicting the ACS using exposed surface area, or quantifying the stealth ability of an aircraft

Manuscript received February 28, 2016, revised May 17, 2016, accepted June 8, 2016. Corresponding author: Y. Huang.

Q. Xu is with College of Electronic and Information Engineering, Nanjing University of Aeronautics and Astronautics, Nanjing, 211106, China, and Department of Electrical Engineering and Electronics, The University of Liverpool, Liverpool, L69 3GJ, UK (e-mail: emxu@foxmail.com).

Y. Huang, Z. Tian, J. Zhou, A. Chen and Y. Zhuang are with the Department of Electrical Engineering and Electronics, The University of Liverpool, Liverpool, L69 3GJ, UK (e-mail: yi.huang@liv.ac.uk; zhihao.tian@liv.ac.uk; jiafeng.zhou@liv.ac.uk).

L. Xing is with College of Electronic and Information Engineering, Nanjing University of Aeronautics and Astronautics, Nanjing, 211106, China. (e-mail: xinglei@nuaa.edu.cn).

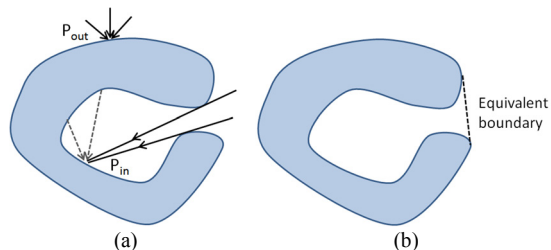


Fig. 1. A perfect absorber of arbitrary (concave) shape, (a) mathematical point of view, (b) physical point of view.

averaged over all incident angles and polarizations. The average absorption coefficient (AAC) can be understood as a system-level parameter to characterize the overall absorptive ability of an arbitrarily shaped object.

By generalizing the idea in [12]-[14], the problem becomes how to obtain the ACS value of an arbitrarily shaped perfect absorber. It has been shown in [10] that the ACS of perfect absorbers with some regular objects can be derived analytically and is found to be a quarter of its surface area. It could be very easy to mistakenly use the overall surface area to calculate the ACS of an arbitrarily shaped perfect absorber. If the OUT shape is concave, because of the shadow, using the overall surface area will give an overestimated value. From a mathematical point of view, the reason is that the shadow will block the incoming wave at some angles which will limit the integral angle region [11, eq. (31)]. This phenomenon is illustrated in Fig. 1(a), at the infinitesimal area of P_{out} , the surface can interact with all the waves coming from outside. However, only the waves from the gap can interact with the absorber at P_{in} , there are no waves coming from the directions in dashed lines. This can also be understood from a physical point of view (boundary condition), an equivalent boundary can be chosen as shown in Fig. 1(b) to short the gap (Huygen's principle). Because not all surfaces can interact with waves coming from all angles (maximum half space), using the surface area to calculate the ACS of a perfect absorber may give an overestimated value.

In this letter, we deal with this problem by calculating the projected area in all angles numerically. For an electrically large perfect absorber, the ACS in each direction is the projected area. A 3D model can be represented by using a point cloud; each point can be projected into a 2D plane; and then a numerical algorithm can be applied to calculate the area of the point cloud in 2D. Thus once the projected area in all directions

is obtained, the averaged value can be calculated which is the reference value in the RC.

The letter is organized in four sections. In Section II, the theory and algorithm are introduced. In Section III, simulations and measurements are performed to validate the results, and finally, discussions and conclusions are given in Section IV.

II. THEORY AND ALGORITHM

A. Theory

Suppose, we have a perfect/ideal electrically large absorber which has the same shape as the OUT and we denote the average ACS value of it as $\langle A_\infty \rangle$, which means it is the theoretical limit (reference value). By comparing the measured ACS ($\langle A_{RC} \rangle$) to $\langle A_\infty \rangle$, the AAC $\langle \alpha \rangle$ can be defined as

$$\langle \alpha \rangle = \langle A_{RC} \rangle / \langle A_\infty \rangle, \quad (1)$$

where $\langle \cdot \rangle$ means the averaged value over all incident angles and polarizations. The value of $\langle \alpha \rangle$ is between 0 and 1. Similarly, the average power scattering coefficient $\langle \Gamma \rangle$ (including reflection and transmission) can be obtained as $\langle \Gamma \rangle = 1 - \langle \alpha \rangle$ [12]-[14].

It is well-known that $\langle A_{RC} \rangle$ can be measured in the RC [1]

$$\langle A_{RC} \rangle = (Q_l^{-1} - Q_u^{-1}) 2\pi V / \lambda, \quad (2)$$

where V is the RC volume, λ is the wave length, Q_l and Q_u are the quality factors (Q factors) of the RC with OUT (load) and without OUT (unload) respectively. Note that the Q factor can be obtained in the frequency domain using Hill's equation $Q = 16\pi^2 V \langle |S_{21,s}|^2 \rangle / \lambda^3$ [1] or in the time domain [1] $Q = \omega \tau_{RC}$ where $S_{21,s}$ is the stirred part of the measured S -parameters [1], ω is the angular frequency and τ_{RC} is the chamber decay time constant [1]. The problem is the determination of $\langle A_\infty \rangle$. For an arbitrarily shaped object, there is no analytical solution but a numerical result can be obtained. For an electrically large perfect absorber, the ACS in each direction is the projected area. As long as we can obtain the projected area in all directions ($A_\infty(\theta, \varphi)$), the averaged value $\langle A_\infty \rangle$ can be obtained.

B. Algorithm

An arbitrarily shaped ideal absorber is shown in Fig. 2(a). A plane wave impinges from a direction (θ, φ) given in a spherical coordinate system. The vectors \hat{r}_p and \hat{r}_q are two unit vectors in the constant phase plane ($\hat{r}_p \perp \hat{r}_q$, $\hat{r}_p \perp \hat{r}$, $\hat{r}_q \perp \hat{r}$). To obtain the projected area, the 3D model is discretized into a point cloud; each point can be projected into the 2D plane by applying $P_{2Dp} = \hat{r}_p \cdot \vec{P}_{3D}$, $P_{2Dq} = \hat{r}_q \cdot \vec{P}_{3D}$ as shown in Fig. 2(b). Next, the 2D plane is discretized into small grids; by counting the grids occupied by the projected points (the shaded grids in Fig. 3(a)), the projected area in 2D can be obtained as shown in Fig. 3(b). By repeating this procedure for each direction (θ, φ) , $A_\infty(\theta, \varphi)$ can be obtained. Because the projected areas in the directions $\vec{r}(\theta, \varphi)$ and $-\vec{r}(\theta, \varphi)$ are the

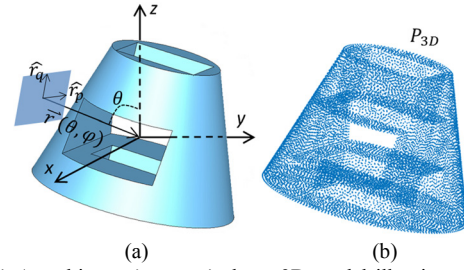


Fig. 2. (a) An arbitrary (concave) shape 3D model illuminated by a plane wave coming from direction (θ, φ) , (b) projected points in 2D.

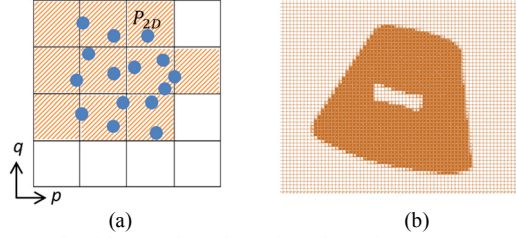


Fig. 3. (a) Grids with 2D points, (b) projected area in 2D.

same, only directions in the hemisphere need to be calculated. This procedure can also be calculated in real-time by using the graphics processing unit (GPU) [15].

After $A_\infty(\theta, \varphi)$ is obtained for each direction (θ, φ) , the average ACS $\langle A_\infty \rangle$ can be obtained as [10]

$$\langle A_\infty \rangle = \frac{\int_0^{2\pi} \int_0^\pi A_\infty(\theta, \varphi) \sin\theta d\theta d\varphi}{\int_0^{2\pi} \int_0^\pi \sin\theta d\theta d\varphi} = \frac{\int_0^{2\pi} \int_0^{\pi/2} A_\infty(\theta, \varphi) \sin\theta d\theta d\varphi}{2\pi} \quad (3)$$

which can be evaluated numerically.

III. SIMULATIONS AND MEASUREMENTS

To verify the accuracy of the algorithm, we use three different shapes to calculate $\langle A_\infty \rangle$ and compare the results with analytical values. It has been found that, for a sphere, a rectangular parallelepiped, and a circular cylinder, $\langle A_\infty \rangle$ is 1/4 of the surface area [11]. Actually, for electrically large objects, as long as the shape is convex, $\langle A_\infty \rangle$ is 1/4 of the surface area (the average projected area theorem) [16], [17]. While for arbitrary (concave) shape object, numerical evaluation of (3) is required.

Three objects are used to verify the numerical procedure as shown in Table I, since the analytical solutions have been found in [10]: a sphere with radius $r = 10$, a cube with edge length $h = 20$, and a cylinder with radius $r = 10$ and height $h = 30$ (units can be arbitrary). They are represented by point clouds. Since the surface areas can be obtained analytically, they can be used as reference values to verify the accuracy of the algorithm. As can be seen, the results are very accurate and the relative errors are smaller than 1%.

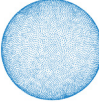
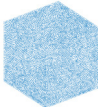

Measurements were performed in the RC at the University of Liverpool for arbitrary (concave) shapes of OUTs. Three measurement scenarios are shown in Fig. 4, the size of the RC is 3.6 m (W) \times 5.8 m (L) \times 4 m (H). Two horn antennas were used (Rohde & Schwarz® HF 906 and SATIMO® SH 2000), 10001 samples of S -parameters in the range of 9.8 GHz \sim 10.2 GHz were collected at each stirrer position. 100 stirrer positions

were used with 3.6 degrees/step, a 10th-order elliptic band pass filter with 10 GHz center frequency and 200 MHz bandwidth was used to filter the S -parameters [18]. The power delay profiles (PDPs) can be obtained from the inverse fast Fourier transform (IFFT) of the filtered S -parameters. It has been found that the ACS measurement in the time domain is more accurate and has lower uncertainties [19] since the early time response, insertion loss of antennas, and cables will not affect the extraction of Q factors. From (2), $\langle A_{RC} \rangle$ can be obtained as [1], [19]

$$\langle A_{RC} \rangle = (\tau_l^{-1} - \tau_u^{-1}) V / c_0, \quad (4)$$

where $c_0 = 3 \times 10^8$ m/s is the speed of light, τ_l is the decay time constant of the RC loaded with the OUT; while τ_u is the decay time constant of the unloaded RC. The least-square fit method [18] is used to extract the decay time constants of PDPs shown in Fig. 7. The results are shown in Table II. For the unloaded RC (including the empty carton used to support the OUT), $\tau_u = 860.4$ ns. Three different positions of the OUT were measured; the maximum difference of the decay time caused by different positions is 4 ns. The maximum relative error of $\langle A_\infty \rangle$ (0.36%) has also been included. From (1), the uncertainty of $\langle \alpha \rangle$ depends on the uncertainties of both $\langle A_{RC} \rangle$ and $\langle A_\infty \rangle$, this gives a maximum uncertainty of 0.02 of $\langle \alpha \rangle$ which is shown in Table II. Three independent measurements could be insufficient to accurately estimate the measurement uncertainty; nevertheless, the maximum differences were used which gave reliable estimated boundaries of the uncertainties.

TABLE I
NUMERICAL VERIFICATION

Shape			
	$r=10$	$h=20$	$r=10$ $h=30$
Number of points	9950	11190	10578
Analytical $\langle A_\infty \rangle$	314.2	600	628.3
Simulated $\langle A_\infty \rangle$	314.5	600.4	630.6
Relative error (%)	0.10	0.07	0.36

Units can be arbitrary.

TABLE II
MEASURED AVERAGE ABSORPTION COEFFICIENTS @ 10 GHz

Scenario	Fig. 4(a)	Fig. 4(b)	Fig. 4(c)
τ_l (ns)	540.1±2	453.7±2	591.5±2
$\langle A_\infty \rangle$ (m ²)	0.23±0.001	0.34±0.001	0.17±0.001
$\langle A_{RC} \rangle$ (m ²)	0.192±0.003	0.290±0.003	0.147±0.002
$\langle \alpha \rangle$	0.83±0.02	0.85±0.01	0.86±0.02

To obtain the AACs, the OUTs are discretized into point clouds. The models are shown in Fig. 5(a) and Fig. 6(a). The

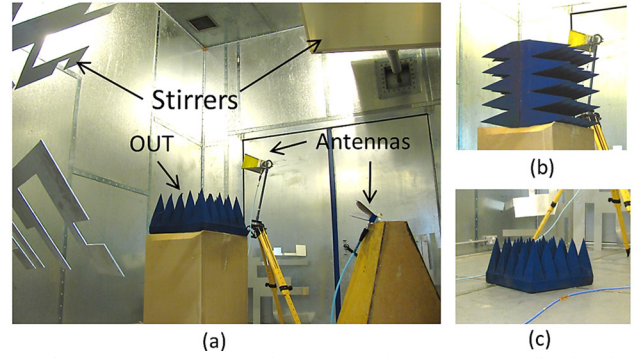


Fig. 4. Three measurement scenarios: (a) one piece of RAM (radio absorbing material) positioned in the center of the RC, (b) back to back two pieces of RAM positioned in the center of the RC and (c) one piece of RAM positioned on the ground.

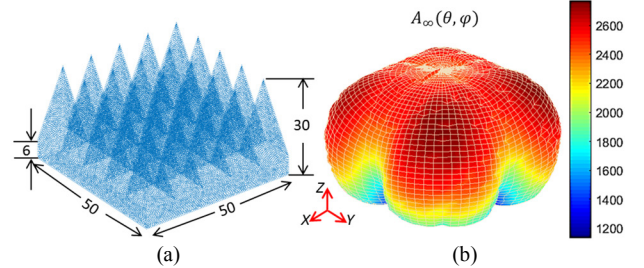


Fig. 5. (a) Point cloud model of a piece of RAM with 62286 points, unit: cm, (b) simulated $A_\infty(\theta, \varphi)$, unit: cm².

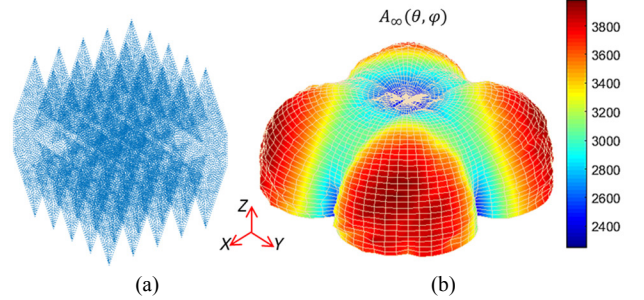


Fig. 6. (a) Point cloud model of back to back two pieces of RAM with 46505 points, (b) simulated $A_\infty(\theta, \varphi)$, unit: cm².

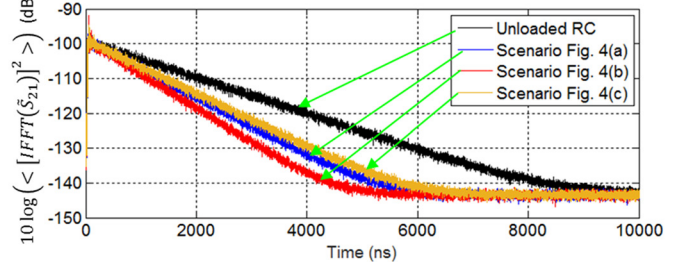


Fig. 7. Measured PDPs of three scenarios, \tilde{S}_{21} represents the filtered S -parameter between two antennas.

simulated $A_\infty(\theta, \varphi)$ patterns with a resolution of 2 degrees/step are given in Fig. 5(b) and Fig. 6(b). By using the two-dimensional trapezoidal rule, the integral in (3) is calculated numerically, thus $\langle A_\infty \rangle$ are obtained. Finally, $\langle \alpha \rangle$ in the three scenarios are obtained using (1). Results are summarized and given in Table II.

At 10 GHz, the OUTs are electrically large. As can be seen in Table II, although the measured average ACSs are different, the AACs $\langle \alpha \rangle$ are very close and not sensitive (but not independent) to the shape and size of the OUT since they are made of the same materials. Note that $\langle \alpha \rangle$ in Fig. 4(b) is larger

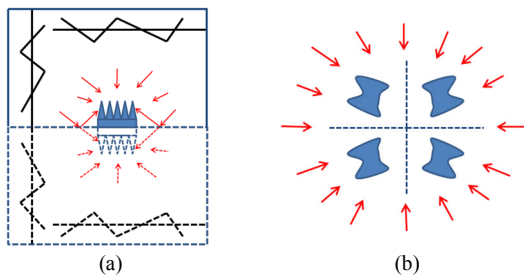


Fig. 8. (a) The effect of the ground plane, images are represented by dashed lines, (b) a general case when the object is positioned at the corner of the RC, waves coming from arbitrary directions are represented by red arrows.

than that in Fig. 4(a), this is because the OUT in Fig. 4(b) has a larger corrugated area ratio (corrugated surface area/overall surface area) than in Fig. 4(a), thus has a larger $\langle \alpha \rangle$. It should be also noted that the ACS in Fig. 4(c) is half of the ACS in Fig. 4(b) but they have similar $\langle \alpha \rangle$. This is because of the image of the ground plane, this effect is shown in Fig. 8(a). However, this does not affect the proposed method. The model with its image can be considered as an integrated model (Fig. 6(a)), after the numerical evaluation of (3), by dividing the result by 2, the final $\langle A_\infty \rangle$ can be obtained. Similarly, if the model is placed close to the corner, as shown in Fig. 8(b), the model and its images can be considered as an integrated model while the ACS needs to be divided by 4 for a 2D problem and divided by 8 for a 3D problem. It can be seen that, when the OUT is far from the boundary of the RC, the image effect is reduced; the overlapping area between the model and its images becomes ignorable. This can also be used to obtain the limit of total scattering cross section (TSCS) of stirrers in [20], since TSCS and ACS are dual quantities. In [20], an equivalent boundary is used to wrap the OUT, and the limit of TSCS (ACS) is a quarter of the equivalent boundary surface area. However, the equivalent boundary with minimum surface area may be hard to find for an arbitrarily shaped OUT (especially when the OUT is close to the boundary of the RC). The numerical procedure in this letter is a general method and does not have this problem, so $\langle A_\infty \rangle$ can be obtained directly without using an equivalent boundary to wrap the OUT.

IV. DISCUSSION AND CONCLUSIONS

In this letter, a general definition of the AAC has been given. For an electrically large perfect absorber, when the shape is convex, from the average projected area theorem [16], [17], $\langle A_\infty \rangle$ is a quarter of the surface area. When the shape is arbitrary, the proposed general method can be applied to obtain $\langle A_\infty \rangle$. By comparing the measured average ACS to $\langle A_\infty \rangle$, the AAC of arbitrarily shaped object can be obtained.

A system-level average absorption/scattering coefficient could be very useful for many applications. The proposed method can be used to compare the absorptive/scattering ability of object with the same material but different shape, evaluate the AAC of a human body, predict the ACS using exposed surface area and even quantify the stealth ability of an aircraft. Note that the size needs to be electrically large when using this method, otherwise $A_\infty(\theta, \varphi)$ needs to be calculated using full wave methods [10].

REFERENCES

- [1] D. A. Hill, *Electromagnetic Fields in Cavities: Deterministic and Statistical Theories*, Piscataway, NJ, USA: IEEE Press, 2009.
- [2] D. Senic, A. Sarolic, Z. M. Joskiewicz and C. L. Holloway, "Absorption cross-section measurements of a human model in a reverberation chamber," *IEEE Trans. EMC*, vol. 58, no.3, pp. 721-728, Jun. 2016.
- [3] I. D. Flintoft, G. C. R. Melia, M. P. Robinson, J. F. Dawson, and A. C. Marvin, "Rapid and accurate broadband absorption cross-section measurement of human bodies in a reverberation chamber," *IOP Meas. Sci. Technol.*, vol. 26, no. 6, pp. 065701-1-065701-9, Jun. 2015.
- [4] I. D. Flintoft, M. P. Robinson, G. C. R. Melia, J. F. Dawson, and A. C. Marvin, "Average absorption cross-section of the human body measured at 1-12 GHz in a reverberant environment: results of a human volunteer study," *IOP Phys. Med. Biol.*, vol. 59, no. 13, pp. 3297-3317, Jul. 2014.
- [5] A. Bamba, D. P. Gaillot, E. Tanghe, G. Vermeeren, W. Joseph, M. Liénard, and L. Martens, "Assessing whole-body absorption cross section for diffuse exposure from reverberation chamber measurements," *IEEE Trans. EMC*, vol. 57, no. 1, pp. 27-34, Feb. 2015.
- [6] G. C. R. Melia, M. P. Robinson, I. D. Flintoft, A. C. Marvin and J. F. Dawson, "Broadband measurement of absorption cross section of the human body in a reverberation chamber," *IEEE Trans. EMC*, vol. 55, no. 6, pp. 1043-1050, Dec. 2013.
- [7] I. D. Flintoft, S. L. Parker, S. J. Bale, A. C. Marvin, J. F. Dawson and M. P. Robinson, "Measured average absorption cross-sections of printed circuit boards from 2 to 20 GHz," *IEEE Trans. EMC*, vol. 58, no. 2, pp. 553-560, Apr. 2016.
- [8] I. D. Flintoft, S. J. Bale, S. L. Parker, A. C. Marvin, J. F. Dawson and M. P. Robinson, "On the measurable range of absorption cross section in a reverberation chamber," *IEEE Trans. EMC*, vol. 58, no. 1, pp. 22-29, Feb. 2016.
- [9] A. Gifuni, G. Ferrara, A. Sorrentino and M. Migliaccio, "Analysis of the measurement uncertainty of the absorption cross section in a reverberation chamber," *IEEE Trans. EMC*, vol. 57, no. 5, pp. 1262-1265, Oct. 2015.
- [10] U. Calberg, P. -S. Kildal, A. Wolfgang, O. Sotoudeh and C. Orlenius, "Calculated and measured absorption cross sections of lossy objects in reverberation chamber," *IEEE Trans. EMC*, vol. 46, no. 2, pp. 146-154, May 2004.
- [11] P. Hallbjörner, U. Carlberg, K. Madsen and J. Anderson, "Extracting electrical material parameters of electrically large dielectric objects from reverberation chamber measurements of absorption cross section," *IEEE Trans. EMC*, vol. 47, no. 2, pp. 291-303, May 2005.
- [12] A. Gifuni, A. Sorrentino, G. Ferrara, M. Migliaccio, A. Fanti and G. Mazzarella, "Measurements on the reflectivity of materials in reverberating chamber," in *Loughborough Antennas & Propagation Conference (LAPC)*, pp. 1-4, Nov. 2011.
- [13] A. Gifuni, "On the measurement of the absorption cross section and material reflectivity in a reverberation chamber," *IEEE Trans. EMC*, vol.51, no.4, pp.1047-1050, 2009.
- [14] A. Gifuni, H. Khenouchi and G. Schirinzì, "Performance of the reflectivity measurement in a reverberation chamber," *Prog. In Electromagn. Research PIER*, vol. 154, pp. 87-100, 2015
- [15] J. M. Rius, M. Ferrando and L. Jofre, "High-frequency RCS of complex radar targets in real-time," *IEEE Trans. Antennas Propagat.*, vol. 41, no. 9, pp. 1308-1319, Sep. 1993.
- [16] V. Vouk, "Projected area of convex bodies," *Nature*, vol. 162, pp. 330-331, Aug. 1948.
- [17] Z. Slepian, "The average projected area theorem-generalization to higher dimensions," arXiv:1109.0595, Nov. 2012.
- [18] C. L. Holloway, H. A. Shah, R. J. Pirkl, K. A. Remley, D. A. Hill and J. Ladbury, "Early time behavior in reverberation chambers and its effect on the relationships between coherence bandwidth, chamber decay time, RMS delay spread, and the chamber buildup time," *IEEE Trans. EMC*, vol. 54, no. 4, pp.717-725, Nov. 2012.
- [19] Z. Tian, Y. Huang, Y. Shen and Q. Xu, "Efficient and accurate measurement of absorption cross section of a lossy object in reverberation chamber using two one-antenna methods," *IEEE Trans. EMC*, vol. 58, no. 3, pp. 686-693, Jun. 2016.
- [20] Q. Xu, Y. Huang, L. Xing, C. Song and M. Stanley, "The limit of the total scattering cross section of electrically large stirrers in a reverberation chamber," *IEEE Trans. EMC*, vol. 58, no. 2, pp. 623-626, Apr. 2016..